

The Role of Mass Asymmetry and Shell Structure in the Evaporation Residues Production

G. Fazio, G. Giardina,* and A. Lamberto
*INFN, Sezione di Catania,
and Dipartimento di Fisica dell'Università di Messina, Italy*

A.I. Muminov and A.K. Nasirov†
Heavy Ion Physics Department, INP, Tashkent, Uzbekistan

U.T. Yakshiev
Theoretical Physics Department, National University of Uzbekistan, Tashkent, Uzbekistan

Yu.Ts. Oganessian, A.G. Popeko, R.N. Sagaidak, and A.V. Yeremin
Flerov Laboratory of Nuclear Reactions, JINR, Dubna, Russia

S. Hofmann
Gesellschaft für Schwerionenforschung mbH, Darmstadt, Germany

F. Hanappe
Université Libre de Bruxelles, Bruxelles, Belgium

L. Stuttgé
Institut de Recherches Subatomiques, Strasbourg, France
(Dated: November 4, 2018)

The effects of the entrance channel and shell structure of reacting nuclei on the experimental evaporation residues have been studied by analysing the $^{40}\text{Ar} + ^{176}\text{Hf}$, $^{86}\text{Kr} + ^{130,136}\text{Xe}$, $^{124}\text{Sn} + ^{92}\text{Zr}$ and $^{48}\text{Ca} + ^{174}\text{Yb}$ reactions leading to the $^{216}\text{Th}^*$ and $^{222}\text{Th}^*$ compound nuclei. The measured excitation function of evaporation residues for the $^{124}\text{Sn} + ^{92}\text{Zr}$ reaction was larger than that for the $^{86}\text{Kr} + ^{130}\text{Xe}$ reaction. The experimental values of evaporation residues in the $^{86}\text{Kr} + ^{136}\text{Xe}$ reaction were about 500 times larger than that in the $^{86}\text{Kr} + ^{130}\text{Xe}$ reaction. These results are explained by the initial angular momentum dependence of the fusion excitation functions calculated in framework of the dinuclear system concept and by the differences in survival probabilities calculated in framework of advanced statistical model. The dependencies of the fission barrier and the Γ_n/Γ_f ratio on the angular momentum of the excited compound nucleus are taken into account.

PACS numbers: 25.70.Gh Fusion and fusion-fission reactions, 25.70.-z Heavy ion induced reactions and scattering, 25.70.Gh Compound nucleus and 27.80.+w $190 \leq A \leq 219$

I. INTRODUCTION

The study of the role of entrance channel in the formation of evaporation residues is an actual problem to establish the optimal conditions for the synthesis of new superheavy elements. Comparison of excitation functions of evaporation residue (ER) measured for different mass-asymmetry reactions but leading to the same compound nucleus (CN) allows us to analyze the importance of the entrance channel effect on the fusion-fission reaction mechanism in collisions of massive nuclei. Often excitation functions of evaporation residues, measured in

various reactions leading to the same compound nucleus, are different not only in the position of the maximum but also in the value of their maximums.

The analysis of data obtained from experiments in GSI (Darmstadt) and Flerov Laboratory of Nuclear Reactions (Dubna) reveals that the maximum value of the ER cross section for $^{40}\text{Ar} + ^{176}\text{Hf}$ [1, 2] is twelve times larger than for $^{86}\text{Kr} + ^{130}\text{Xe}$ [3] and three times larger than for $^{124}\text{Sn} + ^{92}\text{Zr}$ [4]. All of these reactions lead to the same excited $^{216}\text{Th}^*$ compound nucleus. The $^{40}\text{Ar} + ^{176}\text{Hf}$ reaction has a larger mass asymmetry ($\eta_A = (A_2 - A_1)/(A_1 + A_2)$) in comparison with the two others. But intriguing phenomenon is that the measured maximum value of the ER for $^{124}\text{Sn} + ^{92}\text{Zr}$ is four times larger than for $^{86}\text{Kr} + ^{130}\text{Xe}$, nearly at the same E^* value, though the mass asymmetry ($|\eta_A| = 0.148$) of the $^{124}\text{Sn} + ^{92}\text{Zr}$ reaction is smaller than the one of $^{86}\text{Kr} + ^{130}\text{Xe}$ (0.204).

In case of $^{48}\text{Ca} + ^{174}\text{Yb}$ [5] and $^{86}\text{Kr} + ^{136}\text{Xe}$ [3] reactions leading to the excited ^{222}Th compound nucleus,

*Electronic address: giardina@nucleo.unime.it

†Also at Bogoliubov Laboratory of the Theoretical Physics, JINR, Dubna, Russia, and Institut für Theoretische Physik der Justus-Liebig-Universität, Giessen, Germany

the comparison of the measured data on the cross section of evaporation residues does not show strongly the role of mass asymmetry of entrance channel.

The influence of the neutron number on the measured ER was studied in reactions with ^{86}Kr on the ^{130}Xe and ^{136}Xe targets. The difference between the experimental data in above mentioned reactions shows to be connected by the dependence of the strength of quasifission on the entrance channel, namely on the mass asymmetry and shell structure of colliding nuclei.

The entrance channel dependence of the distribution of reaction strength has been studied for three systems, namely $^{32}\text{S} + ^{182}\text{W}$, $^{48}\text{Ti} + ^{166}\text{Er}$, and $^{60}\text{Ni} + ^{154}\text{Sm}$, which all lead to the compound system ^{214}Th in complete fusion reactions [6]. The maximum contribution of complete fusion-fission process to the fission-like cross section is estimated on the basis of expected angle-mass correlations for such reactions. The results show a strong entrance channel dependence as predicted by the extra-push model.

The role of entrance channel effects was studied in [7] where the reactions with ^{40}Ar and ^{84}Kr leading to the same ^{200}Po CN were analysed. Comparison of the measured excitation functions for the isotopes $^{200-xn}\text{Po}$ produced in the $^{40}\text{Ar} + ^{160}\text{Dy}$ and $^{84}\text{Kr} + ^{116}\text{Cd}$ reactions showed that the (Ar, xn) cross sections are larger by factors of $2 \div 4$ than the corresponding (Kr, xn) values. In the experiment of this group, an effect of the entrance channel on the formation and decay of ^{158}Er produced in reactions with either ^{40}Ar and ^{84}Kr , as well as on the de-excitation of compound nucleus by neutron evaporation was not considered [8]. In reactions of massive projectile and target nuclei, the competition between complete fusion and quasifission appears at the stage of CN formation, in addition to the increase of its fission probability. Even in the case of mass-asymmetric collisions, an inhibition of the fusion was recently observed in the experiment by Hinde and his colleagues [9]. The $^{12}\text{C} + ^{204}\text{Pb}$, $^{19}\text{F} + ^{197}\text{Au}$ and $^{30}\text{Si} + ^{186}\text{W}$ reactions leading to the same ^{216}Ra nucleus have been studied. The authors stressed that there is a significant inhibition of the reduced fusion cross section ($\bar{\sigma} = \sigma/\pi\lambda^2$) for reactions with ^{19}F and ^{30}Si , being (0.64 ± 0.09) and (0.57 ± 0.08) , respectively, of those for ^{12}C .

According to the macroscopic dynamical model (MDM) [10] the "extra push" energy, which is needed to transform dinuclear system into compound nucleus, is smaller for asymmetric reaction than for more symmetric one leading to the same compound nucleus. The same effect of the mass asymmetry of the projectile-target pair on the probability of compound nucleus formation is obtained in models based on dinuclear system concept (DNS) [11, 12, 13, 14, 15]. In the DNS concept, fusion is considered as nucleon transfer from the light fragment to the heavy one. From these theories it follows that in reactions with nuclei of symmetric masses there is an inhibition for the fusion, and the quasifission appears as a competing channel with complete fusion.

Quasifission reactions are binary processes that exhibit some of the characteristics of fusion-fission events, such as the full relaxation of the relative kinetic energy and a considerable transfer of mass between the two fragments. The basic difference between fusion-fission and quasifission is that compound nucleus formation is not achieved in the latter mechanism. Anyhow, it is difficult to establish directly in the experiment the origin of fusion-fission fragments.

The aim of this paper is to analyse the role of the mass asymmetry and shell structure in fusion-fission reactions by comparison of the difference between the experimental data for the $^{40}\text{Ar} + ^{176}\text{Hf}$ [1, 2], $^{86}\text{Kr} + ^{130}\text{Xe}$ [3] and $^{124}\text{Sn} + ^{92}\text{Zr}$ [4] reactions leading to the $^{216}\text{Th}^*$ compound nucleus and $^{48}\text{Ca} + ^{174}\text{Yb}$ [5] and $^{86}\text{Kr} + ^{136}\text{Xe}$ [3] reactions leading to the $^{222}\text{Th}^*$ compound nucleus.

A model based on the DNS concept [11] allows one to estimate both contributions of fusion-fission and quasifission processes. It reveals the competition between these processes for a massive system or for a symmetric entrance channel in the case of mid-heavy systems. Calculations based on the DNS-concept show [12, 13, 14, 15, 16] that entrance channel effects are important to describe the experimental data in the case of collisions of massive nuclei. It allows us to estimate the decrease of the fusion probability due to increase of the quasifission process. Calculations of the competition between complete fusion and quasifission process include the peculiarities of shell structure and shape of colliding nuclei. That allows us to reach useful conclusions about the mechanism of the fusion-fission process. As an example, the measured fission excitation function for the $^{40}\text{Ar} + ^{176}\text{Hf}$ reaction obtained from the detection of reaction products of symmetric masses is compared with the calculated fusion excitation function. It should be stressed that those products could be formed not only at the fission of a hot CN but at quasifission of DNS which lives long enough to reach mass equilibration in the subsequent re-separation process.

The dynamical approach to the formation and evolution of DNS [16] in a pair with the advanced statistical model (ASM) [17] shows a good agreement of the calculations with the experiments in a mid-heavy (non-fissile) region of CN [16].

The structure of the article is as follows. Basic features of the dynamical approach and the advanced statistical model are described in Section II. In Section III and IV, we compare the results of calculation with the experimental data and discuss the effect of entrance channel on reaction mechanism. Conclusions are presented in Section V.

II. EVAPORATION RESIDUE PRODUCTION IN THE DNS CONCEPT

According to the DNS concept, evaporation residue production is considered as a three stage process. The

first step is overcoming the Coulomb barrier in motion along the axis connecting nuclear centers by nuclei at the incoming stage of collision, and formation of nuclear composite (molecular-like so-called dinuclear system). This stage is called capture. The second one is transformation of the DNS into more compact compound nucleus in competition with quasifission process. At this stage, the system must overcome the intrinsic barrier (B_{fus}^*) on the potential energy surface during evolution on mass (charge) asymmetry axis. For light and intermediate nuclear systems or for heavy nuclear systems with larger mass asymmetry, this barrier is equal to zero and capture immediately leads to fusion. Therefore, in those cases, the fusion cross section is calculated in the framework of well known models [10, 18, 19, 20]. This barrier will be discussed later. It should be stressed that complete fusion is a transfer of all the nucleons of the projectile (or light nucleus) into the target. Due to large inertia parameter of deformation the change of nuclear shape from the initial state is not so large and the size of overlap region of nuclei is small: it is about 5-6% of the total volume. Therefore, the interacting nuclei retain their shell structure during interaction.

At the third stage, the hot compound nucleus cools down by emission of neutrons and charged particles. There is a chance of nucleus to undergo fission at each step of the de-excitation cascade. Therefore the evaporation residues cross section is determined by the partial fusion cross sections and survival probabilities of the excited compound nucleus:

$$\sigma_{er}(E) = \sum_{\ell=0}^{\ell_d} (2\ell + 1) \sigma_{\ell}^{fus}(E) W_{sur}(E, \ell). \quad (1)$$

Here, the effects connected with the entrance channel are included in the partial fusion cross section $\sigma_{\ell}^{fus}(E)$, which is defined by the product of partial capture cross sections and the related fusion factor (P_{CN}) taking into account competition between complete fusion and quasifission processes:

$$\sigma_{\ell}^{fus}(E) = \sigma_{\ell}^{capture}(E) P_{CN}(E, \ell), \quad (2)$$

$$\sigma_{\ell}^{capture}(E) = \frac{\lambda^2}{4\pi} \mathcal{P}_{\ell}^{capture}(E). \quad (3)$$

Here λ is the de Broglie wavelength of the entrance channel; $\mathcal{P}_{\ell}^{capture}(E)$ is the capture probability which depends on the collision dynamics and is determined by the number of partial waves (ℓ_d) leading to capture.

The potential energy surface is built as a function of the mass (charge) asymmetry and relative distance between centers of nuclei forming DNS. B_{fus}^* is determined by the difference between the maximum value of the driving potential $U(Z, A, R_m)$ and its value at the point corresponding to the initial charge asymmetry of the considered reaction (Fig.1). For example, in top panel of Fig.1, B_{fus}^* is shown for the $^{86}\text{Kr} + ^{130}\text{Xe}$

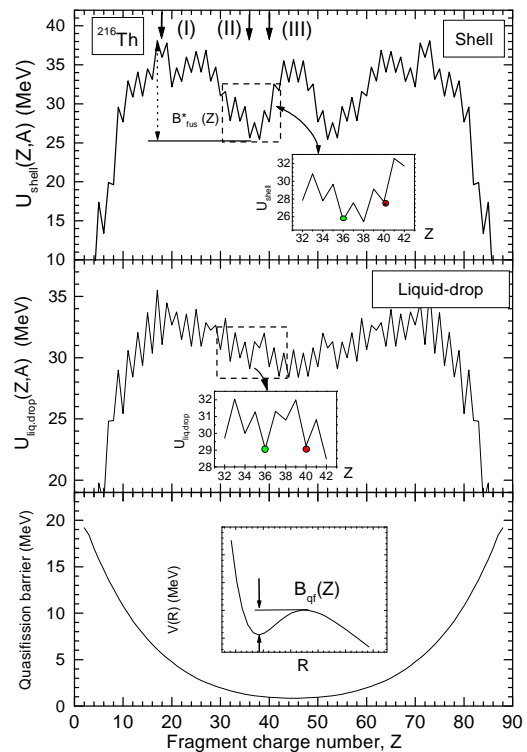


FIG. 1: Driving potential $U(Z, A, R_m; l = 0)$ as a function of the charge number Z of a fragment of a DNS calculated by (4) using binding energies from the nuclear data in [21] (top panel) and those obtained with the liquid-drop model (middle panel). The vertical arrows indicate the initial charge number of light nuclei in the $^{40}\text{Ar} + ^{176}\text{Hf}$ (I) [1, 2], $^{86}\text{Kr} + ^{130}\text{Xe}$ (II) [3] and $^{124}\text{Sn} + ^{92}\text{Zr}$ (III) [4] reactions leading to ^{216}Th . The intrinsic B_{fus}^* (top panel) and quasifission B_{qf} (bottom panel) barriers are shown as a function of the charge number of a DNS fragment.

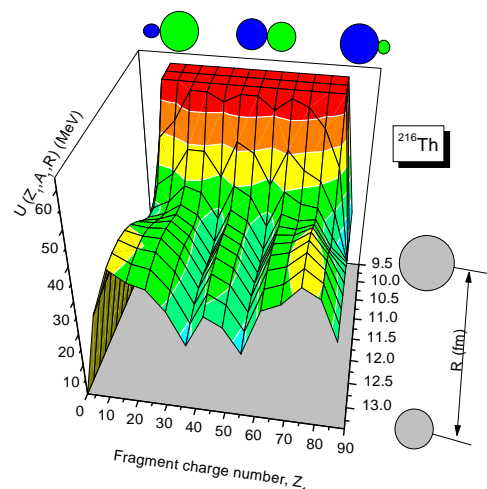


FIG. 2: Potential energy surface $U(Z, A, R; l = 0)$ as a function of the distance R between the centers of the nuclei and charge number Z of a fragment.

reaction. If the excitation energy of dinuclear system, $E_{DNS}^* = E_{c.m.} - V(R_m, \ell)$, is not enough to overcome B_{fus}^* then the dinuclear system may immediately decays into two fragments or its decay occurs after multi-nucleon transfer from heavy fragment into light one. Both of decays are called quasifission. So quasifission fragments can be of different mass asymmetry. Quasifission occurs due to motion along relative internuclear distance R and DNS should overcome the barrier (B_{qf}) defined by the depth of well of $V(R)$ (see insert in bottom panel of Fig. 1).

The $U(Z, A, R_m)$ is extracted from the potential energy surface $U(A, Z; R, \ell)$ (4), which is a function of mass $A = A_1$ (or $A_2 = A_{CN} - A$) and charge $Z = Z_1$ (or $Z_2 = Z_{CN} - Z$) of one of fragments forming the DNS at the values R_m of the internuclear distance corresponding to the minimum of their nucleus-nucleus potential $V(R)$ (8); A_{CN} and Z_{CN} are mass and charge of compound nucleus, respectively. The total potential energy $U(A, Z, R; \ell = 0)$, calculated by this way for the ^{216}Th CN, is presented in Fig.2. The distribution of neutrons between two fragments for the given proton numbers Z and Z_2 (or ratios A/Z and A_2/Z_2 for both fragments) was determined by minimizing the potential $U(A, Z; R)$ as a function of A for each Z :

$$\begin{aligned} U(A, Z; R, \ell) &= U(A, Z, \ell, \beta_1, \alpha_1; \beta_2, \alpha_2) \\ &= B_1 + B_2 + V(Z, \ell, \beta_1, \alpha_1; \beta_2, \alpha_2; R) \\ &\quad - (B_{CN} + V_{CN}(\ell)). \end{aligned} \quad (4)$$

Here, B_1 , B_2 and B_{CN} are the binding energies of the nuclei in DNS and of the CN, respectively, which were obtained from [21, 22]; β_i are the fragment deformation parameters and α_i are the orientations relative to the beam direction; $V_{CN}(\ell)$ is the rotational energy of the compound nucleus. The R_m is the position of this minimum (bottom of the pocket) on the R axis for a given mass of fragment A . The smallest excitation energy value of the CN is determined by the absolute maximum value of the driving potential lying on the way to fusion ($Z = 0$) from the point corresponding to the initial charge asymmetry (Fig.1). The shapes of the potential energy surface and driving potential depend on the orientations of nuclei relative to the axis connecting the centers of interacting nuclei. The presented results were obtained by averaging the contributions of different orientations.

A. Capture

The capture cross section is defined by the number of partial waves which lead colliding nuclei to trap into the well of the nucleus-nucleus potential. The number of the partial waves ℓ_d was obtained by solving the equations of motion for the relative distance and orbital angular momentum taking into account dissipation of collective

kinetic energy [14, 16]:

$$\mu(R(t)) \ddot{\mathbf{R}} + \gamma_R(R(t)) \dot{\mathbf{R}}(t) = -\frac{\partial V(R(t))}{\partial R}, \quad (5)$$

$$\frac{dL}{dt} = \gamma_\theta(R(t)) \left(\dot{\theta} R_{eff}^2 - \dot{\theta}_1 R_{1eff}^2 - \dot{\theta}_2 R_{2eff}^2 \right), \quad (6)$$

where $R(t)$ is the relative motion coordinate; $\dot{\mathbf{R}}(t)$ is the corresponding velocity; $\dot{\theta}$, $\dot{\theta}_1$ and $\dot{\theta}_2$ are angular velocities of the DNS and its fragments, respectively; γ_R and γ_θ are the friction coefficients for the relative motion along R and the tangential motion when two nuclei roll on each other's surfaces, respectively; $V(R)$ is the nucleus-nucleus potential; $\mu(R(t))$ is the reduced mass of the system:

$$\mu(R) = m_0 A_T A_P / A_{tot} \quad (7)$$

where $A_{tot} = A_T + A_P$; m_0 is the nucleon mass; A_T and A_P are mass numbers of the target- and projectile-nucleus, respectively;

$$R_{eff} = \frac{R + R_1 + R_2}{2}, \quad R_{1(2)eff} = \frac{R_{1(2)}}{R_1 + R_2} R,$$

where $R_{1(2)}$ is the nucleus radius.

The friction coefficients γ_R (γ_θ), *i.e.*, the change in the nucleus-nucleus potential and reduced mass of relative motion during the interaction time t , are calculated from the estimation of the coupling term between the relative motion of nuclei and the intrinsic excitation of nuclei [23].

The nucleus-nucleus potential includes Coulomb (V_C), nuclear (V_{nucl}), and rotational (V_{rot}) potentials:

$$V(\mathbf{R}) = V_C(\mathbf{R}) + V_{nucl}(\mathbf{R}) + V_{rot}(\mathbf{R}) + \delta V(R). \quad (8)$$

A change $\delta V(R)$ of the nucleus-nucleus potential and the dynamic contribution $\delta\mu(R)$ to the reduced mass $\mu(R)$ during the interaction time t is taken into account (see Appendix A of paper [14]).

The nucleus-nucleus potential $V(R)$ depends on the mutual orientations of the symmetry axes of the deformed nuclei relative to $\mathbf{R}(t)$. Thus, it is possible to consider contributions to the fusion for different initial orientations of the symmetry axes. The quadrupole (2^+) and octupole (3^-) collective excitations in spherical nuclei are taken into account. Details of this method of calculation are presented in [14].

B. Fusion

The competition between fusion and quasifission is taken into account by the factor $P_{CN}(E, \ell)$ (fusion factor, hereafter) which is calculated in the framework of the statistical model. This way was firstly used in [11]. Validity of using of the statistical method is righteous due to fact that at quasifission a full relaxation of the relative kinetic energy and mass (charge) asymmetry between the two fragments takes place [6]. The statistical

method is acceptable to calculate competition between complete fusion and quasifission processes due to the fact that thermal equilibrium is established in the DNS rather fast, for a few units of 10^{-22} s:

$$\tau_{ther} = 2.6/T_{DNS}^2 \cdot 10^{-22} s.$$

Here T_{DNS} is the effective temperature of DNS: $T_{DNS} = 3.46\sqrt{E_{DNS}^*/A_{tot}}$, where $E_{DNS}^* = E_{c.m.} - V(R_m)$ is excitation energy of DNS; $E_{c.m.}$ is a value of beam energy in the system of the center of mass and $V(R_m)$ is a minimum value of the nucleus-nucleus potential in the potential well.

Duration of the quasifission is one order of magnitude larger than τ_{ther} . It is more than $5 \cdot 10^{-21}$ s which was estimated by the analysis of experimental data on quasifission reactions [24, 25, 26]. The fusion time is longer than quasifission reaction time. The calculation of mass and charge yields in frame of microscopic model showed that formation of DNS with the given mass (charge) asymmetry changes from $5 \cdot 10^{-21}$ s to $9 \cdot 10^{-20}$ s [27, 28, 29]. The experimental data on study of fusion-fission and quasifission reactions induced by ^{48}Ca and ^{58}Fe projectiles on ^{232}Th , ^{238}U , ^{248}Cm and ^{249}Cf targets [30, 31] showed that mass and charge distribution can reach their equilibrium values even in quasifission reactions. It was observed that products far from initial nuclei could be formed not only at the fission of a hot CN but at quasifission of DNS which lives long enough to reach mass equilibration.

Experimentally it is difficult to distinguish between fission of the compound nucleus and quasifission. Only analysis of correlation between reaction fragment mass and angular distributions allows us to estimate a ratio between contributions of quasifission and fusion-fission processes. These theoretical and experimental results on quasifission justify the use of statistical approach to estimate competition of the complete fusion and quasifission processes. Calculation of complete fusion in competition with quasifission can be performed in the framework of statistical methods. The probability of realizing complete fusion is related to the ratio of the level densities, depending on the intrinsic fusion or quasifission barriers, by the expression:

$$P_{CN} = \frac{\rho(E_{DNS}^* - B_{fus}^*)}{\rho(E_{DNS}^* - B_{fus}^*) + \rho(E_{DNS}^* - B_{qf})}, \quad (9)$$

where $\rho(E_{DNS}^* - B_K^*)$ is the level density for the DNS which is calculated on the quasifission and intrinsic fusion barriers ($B_K = B_{qf}, B_{fus}^*$) (all details are in Appendix A of [14]). The final result for the partial fusion cross is obtained by averaging over the contributions of different mutual orientations of the symmetry axes of the reacting nuclei.

C. Survival probability

The advanced statistical model, described in detail in [17, 32, 33], allows us to take into account the dynam-

ical aspects of the fission-evaporation competition during the evolution of the compound nucleus along the de-excitation cascade. The model accounts for the angular momentum and parity coupling; it allows for the neutron, proton, and α -particle multiple emission, as well as for the fission channel and full γ -cascade in the residual nuclei.

Particular attention is devoted to the determination of level densities. These are calculated in the non-adiabatic approach allowing for rotational and vibrational enhancements. These collective effects are gradually removed above a certain energy. In the case of rotational enhancement, this energy is related to the Coriolis force which couples intrinsic and collective motions. The used level densities acquire a dynamic aspect through the dependence of the Coriolis force and of the rotational enhancement on the nuclear shape, which is, in turn, obtained from the classical model of a rotating liquid drop. Intrinsic level densities are calculated using the Ignatyuk approach [34], which takes into account shell structure effects and pairing correlations. Use of the correct level densities is of fundamental importance for the present analysis as they determine the phase space available for each channel, the very essence that governs statistical decay.

In the case of evaporation residue production, one should also carefully consider the low energy level densities since in this energy interval most of the evaporation residues is formed. That is why we use the super-fluid model of the nucleus [35] in our calculations, with the standard value of pairing correction $\Delta = 12/\sqrt{A}$ MeV. The yrast lines are automatically included in our calculations by the requirement that the total excitation energy should be higher than the rotational energy, otherwise the level density is set to zero.

For the fission barriers, we use the predictions of the rotating droplet model (angular momentum dependent) as parameterized by Sierk [36] and allow for angular momentum and temperature fade-out of the shell corrections [17]. This is expressed by the formula for the actual fission barrier used in calculations:

$$B_{fis}(J, T) = c B_{fis}^m(J) - h(T) q(J) \delta W, \quad (10)$$

which includes a dependence on temperature of the compound nucleus

$$h(T) = \begin{cases} 1 & T \leq 1.65 \text{ MeV} \\ k \exp(-mT) & T > 1.65 \text{ MeV}, \end{cases}$$

and

$$q(J) = \{1 + \exp[(J - J_{1/2})/\Delta J]\}^{-1},$$

where $B_{fis}^m(J)$ is the parameterized macroscopic fission barrier [36] depending on the angular momentum J , $\delta W = \delta W_{sad} - \delta W_{gs} \simeq -\delta W_{gs}$ is the microscopic (shell) correction to the fission barrier taken from the tables [22] and the constants for the macroscopic fission barrier

scaling, temperature, and angular momentum dependencies of the microscopic correction are chosen as follows: $c = 1.0$, $k = 5.809$, $m = 1.066 \text{ MeV}^{-1}$, $J_{1/2} = 24\hbar$ for nuclei with $Z \simeq 80\text{--}100$, $\Delta J = 3\hbar$. This procedure allows the shell corrections to become dynamical quantities, also.

Dissipation effects, which delay fission, are treated according to [37, 38]. These include Kramers' stationary limit [39] and an exponential factor applied to Kramers' fission width to account for the transient time, after which the statistical regime is reached. The systematics obtained by Bhattacharya *et al.* [40] allows us to take into account the dependencies of the reduced dissipation coefficient β_{dis} on the incident energy per nucleon ϵ and nucleus mass A

$$\beta_{dis}(\epsilon, A) = a\epsilon + bA^3, \quad (11)$$

where $a = 0.18$, $b = 0.357 \times 10^{-6}$. β_{dis} is the ratio between the friction coefficient γ , which describes the coupling of the fission degree of freedom to the intrinsic degrees of freedom. This ratio characterizes the dissipative and diffusive motion. For the investigated reactions, the β_{dis} values are in $(6 \div 7) \times 10^{21} \text{ s}^{-1}$ range.

In the present ASM calculations, the target-projectile fusion cross section was determined by formula (2). The survival probability W_{sur} is defined by the dependence of fusion cross section on the initial values of the orbital angular momentum, since such a spin distribution affects the fission barrier and the Γ_n/Γ_f ratio that determine the evaporation residue production.

III. COMPARISON OF CALCULATED RESULTS AND EXPERIMENTAL DATA

The difference between measured data on the cross section of evaporation residues for $^{40}\text{Ar} + ^{176}\text{Hf}$ [1, 2], $^{86}\text{Kr} + ^{130}\text{Xe}$ [3] and $^{124}\text{Sn} + ^{92}\text{Zr}$ [4] reactions leading to the heated $^{216}\text{Th}^*$, as well as that for $^{48}\text{Ca} + ^{174}\text{Yb}$ [5] and $^{86}\text{Kr} + ^{136}\text{Xe}$ [3] reactions leading to the heated $^{222}\text{Th}^*$, are explained by the dependencies of fusion excitation functions on the mass asymmetry and shell structure of colliding nuclei and by the dependencies of survival probabilities on the spin distribution of the excited compound nuclei produced in these reactions.

A. The reactions leading to $^{216}\text{Th}^*$

A dependence of the reaction mechanism on the entrance channel was studied in experiments with reactions leading to the same compound nucleus. The experimental data reveal that the maximum value of the ER cross section for $^{40}\text{Ar} + ^{176}\text{Hf}$ (I) [1, 2] is twelve times larger than for $^{86}\text{Kr} + ^{130}\text{Xe}$ (II) [3] and three times larger than for $^{124}\text{Sn} + ^{92}\text{Zr}$ (III) [4] (see Fig.3). The $^{40}\text{Ar} + ^{176}\text{Hf}$ reaction has a larger charge asymmetry ($\eta_A = (A_2 - A_1)/(A_1 + A_2)$) in comparison with the

TABLE I: Charge asymmetry, intrinsic fusion (B_{fus}^*) and quasifission (B_{qf}) barriers, and the fusion factor (P_{CN}) for the reactions leading to $^{216}\text{Th}^*$ CN.

Reactions	η_Z	B_{fus}^* (MeV)	B_{qf} (MeV)	P_{CN}
$^{40}\text{Ar} + ^{176}\text{Hf}$ (I)	0.63	2.31	5.62	0.121
$^{86}\text{Kr} + ^{130}\text{Xe}$ (II)	0.20	12.31	2.35	0.011
$^{124}\text{Sn} + ^{92}\text{Zr}$ (III)	0.15	9.87	1.35	0.051

two others (II,III). This result agrees with the conclusions of MDM [10] and DNS models which state that more asymmetric reactions are favorable for formation of massive compound nucleus. In MDM, "extra push" energy, which is needed to transform dinuclear system into compound nucleus, is smaller for an asymmetric reaction than that for a more symmetric one leading to the same compound nucleus because

$$Z_1^{asym} \cdot Z_2^{asym} < Z_1^{sym} \cdot Z_2^{sym}$$

, if both of reactions lead to the same compound nucleus ($Z_1^{asym} + Z_2^{asym} = Z_1^{sym} + Z_2^{sym}$). The calculated driving potential shows that the barrier B_{fus}^* in the way to fusion (on mass asymmetry axis) is smaller for asymmetric reaction than that for symmetric one; the quasifission barrier is larger for a more asymmetric reaction (see Table I) and as a result the fusion factor P_{CN} becomes larger in this case. As it is seen from Figs.3a and 3b, the excitation function of the capture and fusion for reaction (I) is sufficiently higher than that for reactions (II) and (III), because potential well of entrance channel for the (I) reaction is deeper than that for the others. Therefore, $B_{qf}^{(I)} > B_{qf}^{(II)}$, $B_{qf}^{(III)}$ (see Table I). The smallness of B_{fus}^* for the (I) reaction is connected with the peculiarities of the driving potential (Fig.1).

The evaporation residue excitation functions calculated in this paper using the method presented in Section II are in good agreement with the experimental data (see Fig.3c). In these calculations, the partial cross sections of fusion (2) were used.

It is seen from Fig.3c that the maximum value of the ER cross section for $^{86}\text{Kr} + ^{130}\text{Xe}$ is four times smaller than for $^{124}\text{Sn} + ^{92}\text{Zr}$ near the same value of E_{CN}^* though the former reaction is more asymmetric than latter. This fact was one of the impact points of the presented exploration. This phenomenon is explained by the driving potential calculated using binding energies obtained from the mass table [21]. As one can see in top panel of Fig.1, B_{fus}^* for the $^{86}\text{Kr} + ^{130}\text{Xe}$ reaction is larger than the one of the $^{124}\text{Sn} + ^{92}\text{Zr}$ reaction. Therefore, the fusion excitation function is lower for the former reaction than for the latter. So the observed difference between the excitation functions of evaporation residues for the $^{86}\text{Kr} + ^{130}\text{Xe}$ and $^{124}\text{Sn} + ^{92}\text{Zr}$ reactions is explained by the difference of B_{fus}^* calculated for these reactions using experimental binding energies of fragments. The values of

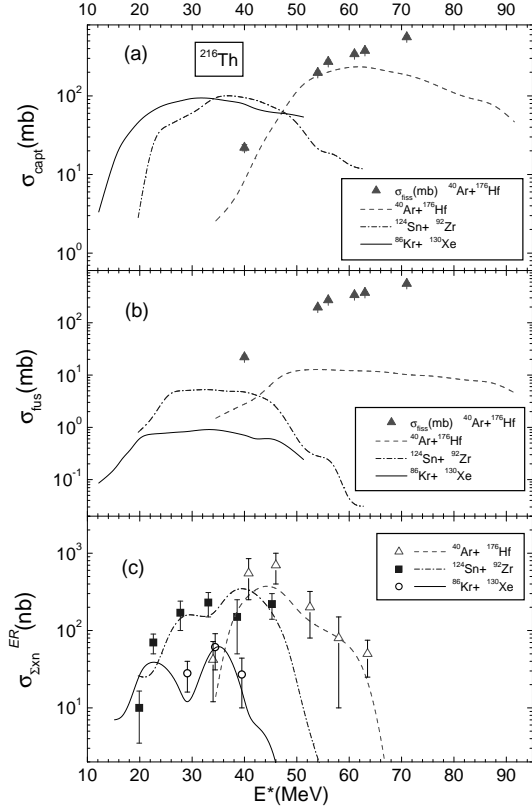


FIG. 3: Comparison of the calculated capture (a), fusion (b) and evaporation residue (c) excitation functions as well as the measured excitation functions of evaporation residue (c) for $^{40}\text{Ar}+^{176}\text{Hf}$ (dashed curve, open up triangles [1, 2]), $^{124}\text{Sn}+^{92}\text{Zr}$ (dash-dotted curve, solid squares [4]), and $^{86}\text{Kr}+^{130}\text{Xe}$ (solid curve, open circles [3]) combinations leading to the $^{216}\text{Th}^*$ CN. The solid triangles in (a) and (b) are the fission excitation functions obtained from the measurements of the two symmetric mass fragments for the $^{40}\text{Ar}+^{176}\text{Hf}$ reaction [2].

B_{fus}^* is small for the region of the reaction (III) due to shell effects contained in the nuclear binding energy.

If the driving potential is calculated using the binding energies B_1, B_2 and B_{CN} obtained in framework of the liquid-drop model, then the intrinsic barriers for these two reactions will be equal $B_{fus}^*(II) \approx B_{fus}^*(III)$ (see the middle panel of Fig.1) and the fusion cross section for the $^{86}\text{Kr}+^{130}\text{Xe}$ reaction will be larger than for the $^{124}\text{Sn}+^{92}\text{Zr}$ reaction due to differences in quasifission barriers. This is in contradiction with experimental data, which indicate that the use of binding energies obtained in the liquid-drop model is not suitable in such an analysis.

The dependence of B_{fus}^* on the orbital angular momentum (Fig.4) affects the partial cross sections of fusion (Fig.5). It is seen from top panel of Fig.4 that the values of driving potential for the fragments of mass less than $A=44$ increase and the part for masses larger than

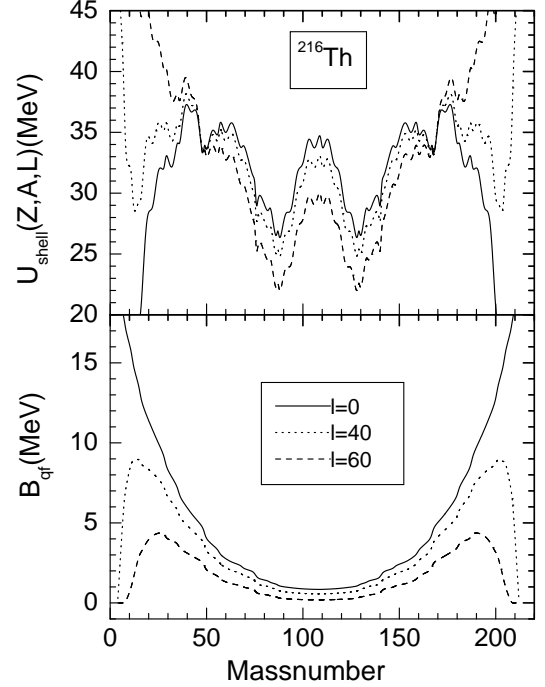


FIG. 4: The dependence of the driving potential (top panel) and quasifission barrier (bottom panel) on orbital angular momentum $\ell(\hbar)$ as a function of the mass of one of fragments for the reactions leading to $^{216}\text{Th}^*$ CN.

$A=44$ decreases by increase of the values of orbital angular momentum. Consequently, values of B_{fus}^* increases by ℓ . But values of quasifission barrier B_{qf} decrease by increasing of the values of orbital angular momentum (bottom panel of Fig.4). As a result the partial fusion cross section decreases by increase of orbital angular momentum. This kind of spin distribution of CN formed in reaction (I) against the beam energy (top panel) has a larger volume in comparison with reactions (II) (middle panel) and (III) (bottom panel). But the volume of the spin distributions of CN corresponding to reaction (III) is larger than that for reaction (II). This is a result of dependence of the partial fusion cross sections $\sigma_{\ell}^{fus}(E)$ (2) on the orbital angular momentum of entrance channel.

As seen in middle panel of Fig.5, for the $^{86}\text{Kr}+^{130}\text{Xe}$ reaction at lowest values of the orbital angular momentum, capture becomes impossible for beam energy larger than 400 MeV. This is connected to the small size of the well in the nucleus-nucleus potential and to the limited value of calculated friction coefficient which leads to a gradual dissipation of relative kinetic energy [23]. Therefore, the dissipation is not enough to trap colliding nuclei in the potential well. At the largest values of beam energy the capture is possible only for high angular momenta (if there is the potential well for the given ℓ). In this case, the formed DNS can exist in a molecular state, forming a super-deformed shape, or it undergoes quasifission because B_{fus}^* increases with angular momentum

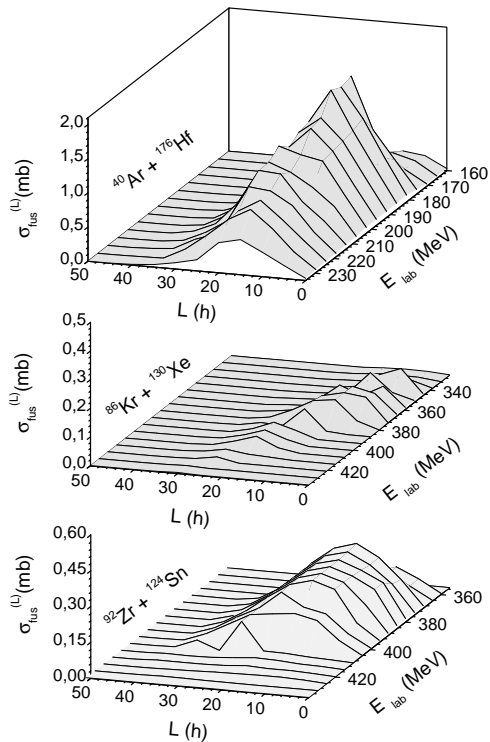


FIG. 5: The calculated spin distribution for the $^{40}\text{Ar}+^{176}\text{Hf}$ (top panel), $^{86}\text{Kr}+^{130}\text{Xe}$ (middle), and $^{124}\text{Sn}+^{92}\text{Zr}$ (bottom) reactions at different beam energies E_{lab} .

of the DNS. Therefore, the maximum of the calculated spin distributions has a tendency to move to larger values of angular momentum at beam energies well above the Coulomb barrier. It can be seen in the spin distributions for $^{86}\text{Kr}+^{130}\text{Xe}$ and $^{124}\text{Sn}+^{92}\text{Zr}$ reactions (Fig.5).

From the analysis of these (I, II and III) reactions leading to $^{216}\text{Th}^*$, one can conclude that:

- the influence of the mass asymmetry and peculiarities of the shell structure on the competition between fusion and quasifission, and on the fusion-fission mechanism is strong;
- the difference between fusion excitation functions deals with the values of B_{fus}^* , which depend on the peculiarities of the nuclear shell structure, and of B_{qf} ; both B_{fus}^* and B_{qf} depend on the entrance channel of reactions under consideration;
- due to the large difference between the Q -values of these three reactions leading to the $^{216}\text{Th}^*$ CN, the centers of their excitation functions (see Fig.3) are placed at different values of excitation energy.

B. Comparison of capture, fusion and fission cross sections for the $^{40}\text{Ar}+^{176}\text{Hf}$ reaction

In these reactions under consideration, the evaporation residue cross sections are several orders of magni-

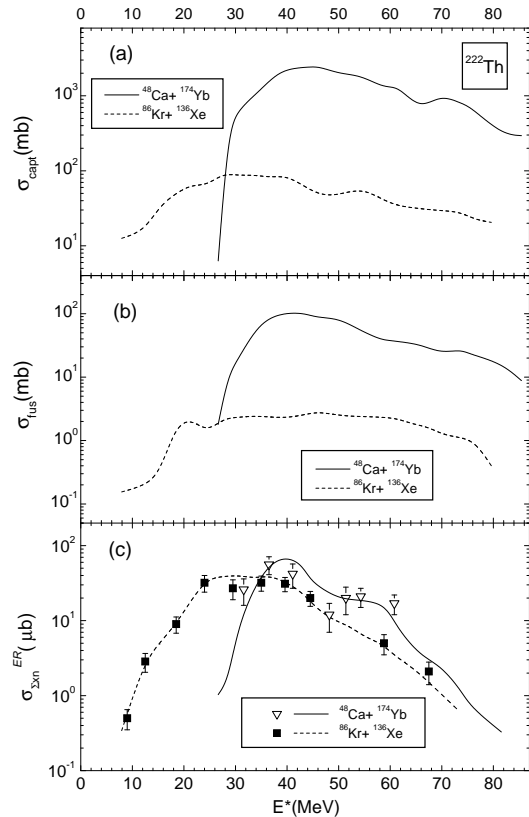


FIG. 6: Comparison of the calculated capture (a), fusion (b) and evaporation residue (c) excitation functions as well as the measured excitation functions of evaporation residue (c) for $^{48}\text{Ca}+^{174}\text{Yb}$ (solid curve, open down triangles [5]) and $^{86}\text{Kr}+^{136}\text{Xe}$ (dashed curve, solid squares [3]) reactions leading to $^{222}\text{Th}^*$.

tude smaller than the fission cross sections (Fig.3). It means that fission cross section is approximately equal to fusion cross section. Comparison of the calculated fusion excitation function and the measured fission excitation function is intriguing when discussing the mechanism of fusion-fission reactions. This has been done for the $^{40}\text{Ar}+^{176}\text{Hf}$ reaction (Fig.3b). In [2], the fission excitation function was obtained from the detection of reaction products of symmetric masses. It should be stressed that those products could be formed not only at the fission of a hot CN but at quasifission of DNS which lives long enough to reach mass equilibration. Experimentally it is difficult to distinguish between fission of the compound nucleus and quasifission. In [16], the calculations showed that the contribution of quasifission is increased with beam energy above the fusion barrier. For this reason, the measured fission data in the $^{40}\text{Ar}+^{176}\text{Hf}$ reaction [2] are closer to the calculated excitation function of capture (Fig.3a) that is a sum of fusion and quasifission cross sections.

Therefore, the fact that the measured fission cross sec-

tion is higher than the calculated fusion cross section (Fig.3b) could be explained by the sizeable contribution of quasifission products to the measured fission data [2]. Appearance of difference between the measured fission and theoretical capture cross sections at energies higher than $E^* = 55$ MeV means that events of capture accompanied by the pre-equilibrium emission of neutrons, protons and α - particles from fragments were not taken into account in the model under consideration.

C. The reactions leading to $^{222}\text{Th}^*$

The maximum of the experimental excitation functions of evaporation residues for $^{48}\text{Ca} + ^{174}\text{Yb}$ (IV) [5] is higher than that for $^{86}\text{Kr} + ^{136}\text{Xe}$ (V) [3] (Fig.6c). This fact can be explained by the large fusion cross sections at excitation energies E^* higher than 24 MeV (Fig.6b). These reactions lead to the $^{222}\text{Th}^*$ CN. Excitation functions of capture and fusion for the $^{48}\text{Ca} + ^{174}\text{Yb}$ reaction are more than one order of magnitude higher than for the $^{86}\text{Kr} + ^{136}\text{Xe}$ reaction.

In Table II, we report the values of the charge asymmetry, intrinsic fusion barrier and quasifission barrier for such two reactions leading to the $^{222}\text{Th}^*$ CN. At excitation energies E^* of the $^{222}\text{Th}^*$ CN lower than about 30 MeV, the excitation functions of capture, fusion and evaporation residue go down for the $^{48}\text{Ca} + ^{174}\text{Yb}$ reaction. This energy corresponds to the Coulomb barrier. Because the Q_{gg} -value for this reaction (-118.35 MeV) is not as low as for the $^{86}\text{Kr} + ^{136}\text{Xe}$ (-186.88 MeV) reaction, the subbarrier region of fusion for the $^{48}\text{Ca} + ^{174}\text{Yb}$ reaction is placed at $E^* < 30$ MeV.

By considering the spin distributions of the two reactions leading to $^{222}\text{Th}^*$ CN, we find a higher contribution to the fission process for the $^{48}\text{Ca} + ^{174}\text{Yb}$ reaction caused by the spin distribution peaked at higher J spin values. As one can see, the spin distribution of CN formed in the $^{48}\text{Ca} + ^{174}\text{Yb}$ reaction against the beam energy (Fig.7, top panel) has a larger volume than that of the $^{86}\text{Kr} + ^{136}\text{Xe}$ reaction (bottom panel).

From calculations of survival probability, we find that in the range of excitation energy between 40 and 60 MeV of $^{222}\text{Th}^*$, and for various steps of the de-excitation cascade, the Γ_n/Γ_f ratio values for the $^{48}\text{Ca} + ^{174}\text{Yb}$ reaction are much lower than those for the $^{86}\text{Kr} + ^{136}\text{Xe}$ reaction. The compound nucleus $^{222}\text{Th}^*$ formed in these reactions at the same excitation energy E^* has different spin distributions which are caused by the dynamical effects in the entrance channel of the two reactions. Due to dependence of fissility on spin distribution in ASM calculation, the evaporation residue have different cross sections. The ratio $(\Gamma_n/\Gamma_f)_{(V)}/(\Gamma_n/\Gamma_f)_{(IV)}$ of the Γ_n/Γ_f values for the $^{48}\text{Ca} + ^{174}\text{Yb}$ and $^{86}\text{Kr} + ^{136}\text{Xe}$ reactions at each step of de-excitation cascade ranges between 2.5 and 6.6×10^4 . Even if in such an energy range the fusion cross section for the $^{48}\text{Ca} + ^{174}\text{Yb}$ reaction is about 1-2 orders of magnitude higher than that for the ^{86}Kr

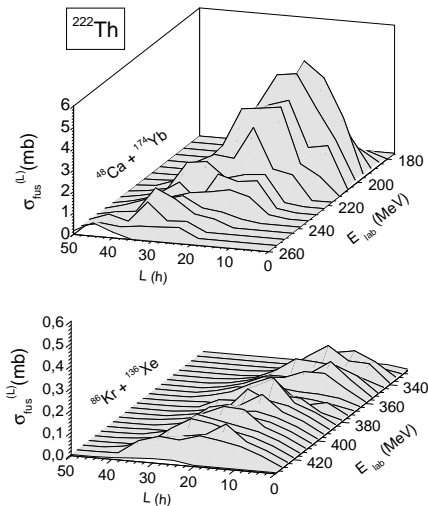


FIG. 7: Spin distribution for $^{48}\text{Ca} + ^{174}\text{Yb}$ (top panel) and $^{86}\text{Kr} + ^{136}\text{Xe}$ (bottom panel) reactions at different beam energies E_{lab} .

TABLE II: Charge asymmetry, intrinsic fusion (B_{fus}^*) and quasifission (B_{qf}) barriers and the fusion factor (P_{CN}) for the reactions leading to $^{222}\text{Th}^*$ CN.

Reactions	ηZ	B_{fus}^* (MeV)	B_{qf} (MeV)	P_{CN}
$^{48}\text{Ca} + ^{174}\text{Yb}$ (IV)	0.56	3.20	5.37	0.065
$^{86}\text{Kr} + ^{136}\text{Xe}$ (V)	0.20	7.52	4.05	0.027

+ ^{136}Xe reaction, the survival probability $W_{sur}(\Gamma_n/\Gamma_f)$ makes the values of the ER cross section for $^{48}\text{Ca} + ^{174}\text{Yb}$ reaction only a factor 2-4 times higher than the ER values of $^{86}\text{Kr} + ^{136}\text{Xe}$.

The analysis of the $^{48}\text{Ca} + ^{174}\text{Yb}$ and the $^{86}\text{Kr} + ^{136}\text{Xe}$ reactions leading to $^{222}\text{Th}^*$ CN shows that:

- influence of the mass asymmetry and peculiarities of the shell structure on the competition between fusion and quasifission mechanism is strong. Nevertheless the comparison of the measured data on the cross section of evaporation residues does not reflect the role of mass asymmetry of entrance channel. The large difference between the fusion cross sections was compensated by the different fissility of nuclei formed in these reactions at various step of de-excitation cascade;

- the difference between fusion excitation functions deals with the values of B_{fus}^* and difference between survival probabilities is connected with the dependence of fusion cross sections on the orbital angular momentum in the entrance channel of reactions under consideration.

IV. COMPARISON OF REACTIONS INDUCED BY ^{86}Kr ON THE ^{130}Xe AND ^{136}Xe TARGETS

Another interesting phenomenon which was observed in the comparison of the experimental data for reactions induced by the ^{86}Kr projectile on the ^{130}Xe and ^{136}Xe targets is that the ER cross section in $^{86}\text{Kr} + ^{130}\text{Xe}$ (II) was about 500 times smaller than that in $^{86}\text{Kr} + ^{136}\text{Xe}$ (V) (Fig.8c). The experimental and theoretical excitation functions presented in Fig.8c are the sum of the evaporation residues along the de-excitation cascade for the neutron emission from $^{216}\text{Th}^*$ and $^{222}\text{Th}^*$ CN formed in these reactions, respectively. It is clear that these differences are caused by the excess number of neutrons in the ^{136}Xe target in comparison with the ^{130}Xe one.

As a result we obtain differences in two characteristics of the fusion-fission mechanism:

- the fusion cross section calculated using the model based on DNS concept [14, 16] for the reaction $^{86}\text{Kr} + ^{130}\text{Xe}$ is much smaller than the one for $^{86}\text{Kr} + ^{136}\text{Xe}$ (Fig.8b). Therefore, the volume of spin distribution of CN formed in the former reaction against the beam energy is smaller than that for the last reaction (Fig.9). This is because for the $^{86}\text{Kr} + ^{136}\text{Xe}$ reaction the intrinsic fusion barrier is smaller and the quasifission barrier is larger than those for the $^{86}\text{Kr} + ^{130}\text{Xe}$ reaction (see Tables I and II);

- the survival probability (W_{sur}) decreases along the steps of the $^{216}\text{Th}^*$ de-excitation cascade, while W_{sur} increases along the steps of the $^{222}\text{Th}^*$ cascade. This is because the shell corrections, in average, decrease for the intermediate excited nuclei after $1n, 2n \dots xn$ emissions from $^{216}\text{Th}^*$, whereas the shell corrections of the excited nuclei increase after the analogous neutron emission from $^{222}\text{Th}^*$. Notice concerning to the excitation energy of the initial compound nucleus, the ER production is more sensitive to the last step of the de-excitation cascade. Moreover, we have to note that at each step ($1n, 2n, 3n \dots xn$) of the de-excitation cascade of the initial compound nucleus, the neutron separation energy S_n at each step of the $^{222}\text{Th}^*$ decay chain is about 1-2 MeV lower than that at the analogous step of the neutron emission from $^{216}\text{Th}^*$. By comparing the Γ_n/Γ_f values at each step of the cascade of $^{222}\text{Th}^*$ and $^{216}\text{Th}^*$, at the same excitation energy of the CN, we find that $(\Gamma_n/\Gamma_f)_{^{222}\text{Th}^*}$ are always much larger than $(\Gamma_n/\Gamma_f)_{^{216}\text{Th}^*}$. In particular, the $(\Gamma_n/\Gamma_f)_{^{222}\text{Th}^*}/(\Gamma_n/\Gamma_f)_{^{216}\text{Th}^*}$ ratio ranges between 2.7×10^4 and 9.1×10^5 for the $4n$ -channel. Since large Γ_n/Γ_f values correspond to a large evaporation residue cross section, the excess number of neutrons increases the survival probability in the $^{86}\text{Kr} + ^{136}\text{Xe}$ reaction in comparison with the $^{86}\text{Kr} + ^{130}\text{Xe}$ one.

V. CONCLUSIONS

The role of the entrance channel in fusion-fission reactions was studied intending to account for the differ-

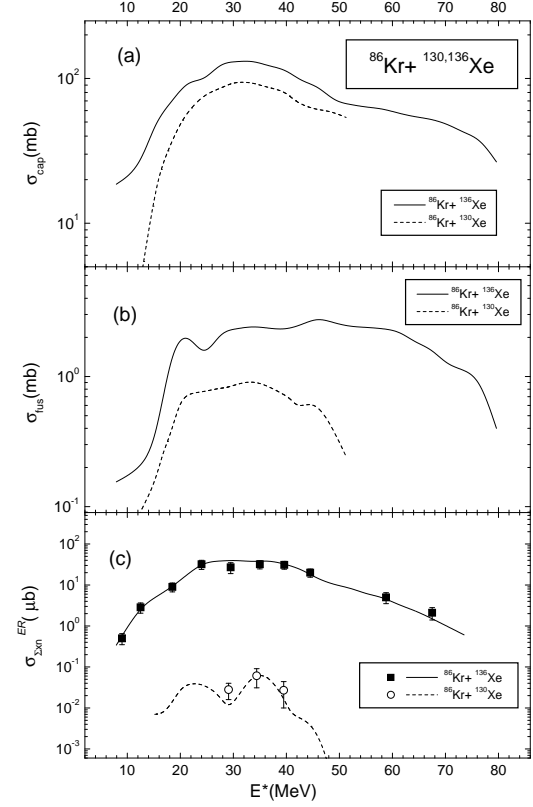


FIG. 8: Comparison of the calculated capture (a), fusion (b) and evaporation residue (c) excitation functions as well as the measured excitation functions of evaporation residue (c) for the $^{86}\text{Kr} + ^{136}\text{Xe}$ (solid curve, solid squares [3]) and $^{86}\text{Kr} + ^{130}\text{Xe}$ (dashed curve, open circles [3]) reactions.

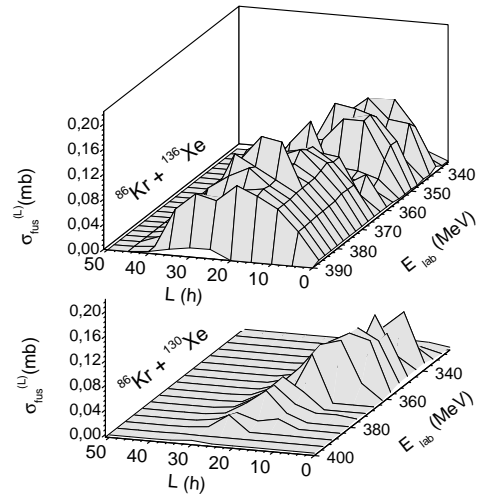


FIG. 9: Spin distribution for the $^{86}\text{Kr} + ^{136}\text{Xe}$ (top panel) and $^{86}\text{Kr} + ^{130}\text{Xe}$ (bottom panel) reactions at different beam energies E_{lab} .

ence between the experimental data for the $^{40}\text{Ar} + ^{176}\text{Hf}$ [1, 2], $^{86}\text{Kr} + ^{130}\text{Xe}$ [3] and $^{124}\text{Sn} + ^{92}\text{Zr}$ [4] reactions leading to the $^{216}\text{Th}^*$ compound nucleus, and the $^{48}\text{Ca} + ^{174}\text{Yb}$ [5], $^{86}\text{Kr} + ^{136}\text{Xe}$ [3] reactions leading to the $^{222}\text{Th}^*$ compound nucleus. The results of calculations in the framework of the DNS concept [14] for the fusion cross sections, and advanced statistical model [17, 32, 33] for the total evaporation residue cross sections have been compared with the measured experimental data for these reactions. From the analysis of the experimental data four phenomena were studied:

i) Among reactions leading to $^{216}\text{Th}^*$, $^{40}\text{Ar} + ^{176}\text{Hf}$ has more larger evaporation residues in comparison with two others: $^{86}\text{Kr} + ^{130}\text{Xe}$ and $^{124}\text{Sn} + ^{92}\text{Zr}$. This result affirms conclusions of macroscopic dynamical and DNS models which state that more asymmetric reactions are favorable to formation of massive compound nucleus. In MDM, "extra push" energy, which is needed to transform dinuclear system into compound nucleus, is smaller for asymmetric reaction than for more symmetric one. The "extra push" energy in MDM [10] and the intrinsic fusion barrier B_{fus}^* in DNS concept [11], (both of which are a hindrance to fusion) are smaller for an asymmetric reaction than for more symmetric one leading to the same compound nucleus (top panel, Fig.1).

ii) One of the unexpected phenomenon is that the measured maximum value of the ER cross section for $^{86}\text{Kr} + ^{130}\text{Xe}$ (II) is four times smaller than that for $^{124}\text{Sn} + ^{92}\text{Zr}$ (III), nearly at the same E^* value. This result is in opposite tendency to the conclusions of MDM and DNS models. The observed difference between the excitation functions of evaporation residues for the $^{86}\text{Kr} + ^{130}\text{Xe}$ and $^{124}\text{Sn} + ^{92}\text{Zr}$ reactions is explained by the difference of B_{fus}^* calculated for these reactions using experimental binding energies of fragments [21]. As one can see in top panel of Fig.1, B_{fus}^* for the $^{86}\text{Kr} + ^{130}\text{Xe}$ reaction is larger than that of the $^{124}\text{Sn} + ^{92}\text{Zr}$ reaction. Therefore, the fusion excitation function is lower for the former reaction than for the latter. The calculated partial cross sections of fusion depend on these intrinsic fusion and quasifission barriers. The volume under surface $\sigma_{fus}^{(L)}(E)$ calculated against beam energy for the $^{86}\text{Kr} + ^{130}\text{Xe}$ reaction is smaller than that for the $^{124}\text{Sn} + ^{92}\text{Zr}$ reaction (Fig.5). This created the necessary prerequisites to obtain larger cross sections of the evaporation residue for the latter reaction in comparison with former one. The calculated results are in good agreement with the experimental data.

If driving potential is calculated using binding energies of liquid-drop model (see middle panel of Fig.1), the intrinsic fusion barriers B_{fus}^* for the $^{86}\text{Kr} + ^{130}\text{Xe}$ and $^{124}\text{Sn} + ^{92}\text{Zr}$ reactions are almost the same and the fusion cross section for the former reaction will be larger than for the latter due to differences in quasifission barriers. That would be in contradiction to the experimental data.

iii) The maximum of the experimental excitation func-

tions of evaporation residues for $^{48}\text{Ca} + ^{174}\text{Yb}$ (IV) [5] is higher than that for $^{86}\text{Kr} + ^{136}\text{Xe}$ (V) [3] (Fig.6c). This fact can be explained by the large fusion cross section at excitation energies $E^* > 25$ MeV (Fig.6b). These reactions lead to the $^{222}\text{Th}^*$ CN. Excitation functions of capture and fusion for the $^{48}\text{Ca} + ^{174}\text{Yb}$ reaction are more than one order of magnitude higher than for the $^{86}\text{Kr} + ^{136}\text{Xe}$ reaction. But due to strong dependence of the various steps of the de-excitation cascade on the spin distribution of hot and rotated compound nuclei: the values of the Γ_n/Γ_f ratio for the $^{48}\text{Ca} + ^{174}\text{Yb}$ reaction are much lower than those for the $^{86}\text{Kr} + ^{136}\text{Xe}$ reaction. The two different entrance channels does not produce the same evaporation residue cross section due to a different fissility of the compound nucleus $^{222}\text{Th}^*$. Different spin distributions $\sigma_{fus}^{(L)}$ are caused by the dynamical effects in the entrance channel of the two very different reactions. Due to dependence of fissility on spin distribution in ASM calculation, the evaporation residues have different cross sections.

The comparison of the measured data on the cross section of evaporation residues does not reflect the role of mass asymmetry of entrance channel (Fig.6c). The large difference between the fusion cross sections was compensated by the different fissility of nuclei formed in these reactions at various steps of de-excitation cascade.

iv) Another interesting phenomenon which was observed in the comparison of the experimental data for reactions induced by the ^{86}Kr projectile on the ^{130}Xe and ^{136}Xe targets is that the ER cross section in $^{86}\text{Kr} + ^{130}\text{Xe}$ (II) was about 500 times smaller than that in $^{86}\text{Kr} + ^{136}\text{Xe}$ (IV) (Fig.8c). The experimental and theoretical excitation functions presented in Fig.8c are the sum of the evaporation residues along the de-excitation cascade for the $^{86}\text{Kr} + ^{130}\text{Xe}$ and $^{86}\text{Kr} + ^{136}\text{Xe}$ reactions. These differences are caused by the excess number of neutrons in the ^{136}Xe target in comparison with ^{130}Xe one. Analysing the mechanism of these reactions, we conclude that due to smallness of intrinsic fusion barrier and largeness of quasifission barrier, capture and fusion cross sections of reaction with the ^{136}Xe target is larger than that the ^{130}Xe one (see Tables I and II). The excess number of neutrons increases the survival probability in the $^{86}\text{Kr} + ^{136}\text{Xe}$ reaction due to increase of values of the Γ_n/Γ_f ratio in comparison with $^{86}\text{Kr} + ^{130}\text{Xe}$ reaction.

To analyse fusion-fission process, the fission cross sections presented in [2] for the $^{40}\text{Ar} + ^{176}\text{Hf}$ reaction were compared with the calculated fusion and capture cross sections. The calculated capture cross sections are in agreement with the measured fission data [2] up to excitation energies E^* of about 54 MeV (Fig.3a). Due to sizeable contribution of quasifission products to the measured fission data [2], the last are larger than the calculated fusion cross section (Fig.3b). The deviation of the calculated capture cross sections from the measured fission data at $E^* > 54$ MeV is connected to the fact that the pre-equilibrium emission of neutrons, protons and α -particles from fragments were not taken into account in

the model under consideration.

In summary, the difference between measured data on the cross section of evaporation residues for reactions leading to the same compound nuclei can be explained by the difference in the excitation functions of fusion or survival probability of the excited compound nucleus. Decrease of fusion cross sections is connected by increase of events coming from the quasifission process. Competition between complete fusion and quasifission depends on the dynamics of the entrance channel and the nuclear shell structure for colliding nuclei. The formation of a compound nucleus at low excitation energy does not ensure the production of evaporation residues with a larger cross section.

Acknowledgments

This work was performed partially under the financial support of the RFBR (Grant No. 99-02-16447)

and INTAS (Grant No. 991-1344). We are grateful to Profs. R.V. Jolos, V.V. Volkov and W. Scheid; Drs. G.G. Adamian and N.V. Antonenko for the helpful discussions. One of the authors (A.K.N.) thanks the Heisenberg-Landau Program for support while staying at the GSI, and RFBR (Grant No. 01-02-16033) for financial support. Authors (A.I.M and A.K.N.) are grateful to the STCU Uzb-45, Uzbekistan State Scientific-Technical Committee (Grant No. 7/2000) and Fund of Uzbek Academy of Science for Support of Basic Research (No. 45-00) for partial support. A.K.N. would like to express his gratitude for the warm hospitality during his stay at GSI, Giessen Justus-Liebig University (Germany), and Università di Messina (Italy). R.N.S. and A.K.N. are also grateful to the Fondazione Bonino-Pulejo (FBP) of Messina for the support received in the collaboration with the Messina group.

-
- [1] D. Vermeulen, H.-G. Clerc, C.-C. Sahn, K.-H. Schmidt, J.G. Keller, G. Münzenberg, W. Reisdorf, *Z. Phys. A* **318**, 157 (1984).
- [2] H.-G. Clerc, J.G. Keller, C.-C. Sahn, K.-H. Schmidt, H. Schulte, D. Vermeulen, *Nucl. Phys. A* **419**, 571 (1984).
- [3] Yu.Ts. Oganessian, A.Yu. Lavrentev, A.G. Popeko, R.N. Sagaidak, A.V. Yeremin, S. Hofmann, F.P. Heßberger, V.Ninov, Ch. Stodel, *JINR FLNR Scientific Report 1995-1996. Heavy Ion Physics*, B.I. Pustylnik (ed.), p. 62 (JINR, E7-97-206, Dubna, 1997).
- [4] C.-C. Sahn, H.-G. Clerc, K.-H. Schmidt, W. Reisdorf, P. Armbruster, F.P. Heßberger, J.G. Keller, G. Münzenberg, D. Vermeulen, *Nucl. Phys. A* **441**, 316 (1985).
- [5] R.N. Sagaidak, et al. *JINR FLNR Scientific Report 1997-1998. Heavy Ion Physics*, A.G. Popeko (ed.), p. 60 (JINR, E7-2000-232, Dubna, 2000).
- [6] B.B. Back, P.B. Fernandez, B.G. Glagola, D. Henderson, S. Kaufman, J.G. Keller, S.J. Sanders, F. Videbk, T.F. Wang, and B.D. Wilkins, *Phys. Rev. C* **53**, 1734 (1996).
- [7] R. L. Hahn, K. S. Toth, Y. LeBeyec, B. Lagarde, M. W. Guidry, *Phys. Rev. C* **36**, 2132 (1987).
- [8] R. L. Hahn, K. S. Toth, C. Cabot, H. Gauvin, Y. LeBeyec, *Phys. Rev. Lett.*, **42** 218 (1979).
- [9] A.C. Berriman, D.J. Hinde, M. Dasgupta, C.R. Morton, R.D. Butt and J.O. Newton, *Nature* **413**, 144 (2001).
- [10] J.P. Blocki, H. Feldmeier, W.J. Swiatecki, *Nucl. Phys. A* **459**, 145 (1986).
- [11] V.V. Volkov, N.A. Antonenko, E.A. Cherepanov, A.K. Nasirov, V.P. Permjakov, *Phys. Lett. B* **319**, 425 (1993); *Phys. Rev. C* **51**, 2635 (1995).
- [12] E.A. Cherepanov, V.V. Volkov, N.A. Antonenko, A.K. Nasirov, *Nucl. Phys. A* **459**, 145 (1996).
- [13] G.G. Adamian, N.A. Antonenko, W. Scheid, V.V. Volkov, *Nucl. Phys. A* **633**, 409 (1998).
- [14] G. Giardina, S. Hofmann, A.I. Muminov, A.K. Nasirov, *Eur. Phys. J. A* **8**, 205 (2000).
- [15] E.A. Cherepanov, *International Conference on Nuclear Physics "Shells-50", Dubna, Russia, 1999*, Yu.Ts. Oganessian, R. Kalpakchieva (eds.), p. 266 (World Scientific, Singapore, 2000).
- [16] G. Giardina, F. Hanappe, A.I. Muminov, A.K. Nasirov, L. Stuttgé, *Nucl. Phys. A* **671**, 165 (2000).
- [17] A. D'Arrigo, G. Giardina, M. Herman, A.V. Ignatyuk, A. Taccone, *J. Phys. G* **20**, 365 (1994).
- [18] W.J. Swiatecki, *Phys. Scr.*, **24**, 113 (1981); *Nucl. Phys. A* **376**, 275 (1982).
- [19] K.T.R. Davies, A.J. Sierk, J.R. Nix, *Phys. Rev. C* **28**, 679 (1983).
- [20] P. Fröbrich, *Phys. Rep.* **116**, 337 (1984); *Phys. Lett. B* **215**, 36 (1988).
- [21] G. Audi, A.H. Wapstra, *Nucl. Phys. A* **595**, 509 (1995).
- [22] P. Möller, J.R. Nix, *Atom. Data and Nucl. Data Tabl.* **39**, 213 (1988).
- [23] G.G. Adamian, R.V. Jolos, A.I. Muminov, A.K. Nasirov, *Phys. Rev. C* **56**, 373 (1997).
- [24] J. Velkovska, C. R. Morton, R. L. McGrath, P. Chung, and I. Diószegi, *Phys. Rev. C* **59**, 1506 (1999).
- [25] D.J. Hinde, D. Hilsher, H. Rossner, B. Gebauer, M. Lehmann, and M. Wilpert, *Phys. Rev. C* **45**, 1229 (1992).
- [26] K. Siwek-Wilczynska, J. Wilczynski, R.H. Siemssen, and H.W. Wilschut, *Phys. Rev. C* **51**, 2054 (1995).
- [27] G.G. Adamian, G. Giardina, A.I. Muminov, and A.K. Nasirov, In *Contribution of International Conference of Fission Dynamics*, Obninsk, 1999.
- [28] G.G. Adamian, N.V. Antonenko, W. Scheid, *Nucl. Phys. A* **618**, 176-198 (1997).
- [29] R. Butsch, D.J. Hofman, C.P. Montoya, P. Paul, and M. Thoennessen, *Phys. Rev. C* **44**, 1515 (1991).
- [30] S. A.A. Bogatchev, et al., In: *Proc. of the International Conference on Nuclear Physics at Border Lines May 21-24, 2001 Lipari (Messina), Italy*, eds. G.Fazio, G.Giardina, F.Hanappe, G.Imme, N.Rowley. World Sci-

- entific, Singapore, p.56-59, 2002.
- [31] M.G. Itkis, et al., In:Proc. of the International Conference on Nuclear Physics at Border Lines, May 21-24, 2001 Lipari (Messina), Italy, eds. G.Fazio, G.Giardina, F.Hanappe, G.Imme, N.Rowley. World Scientific, Singapore, p.146-156, 2002.
- [32] A. D'Arrigo, G. Giardina, M. Herman, and A. Taccone, Phys. Rev. C **46**, 1437 (1992).
- [33] R.N. Sagaidak, V.I. Chepigin, A.P. Kabachenko, J. Roháč, Yu.Ts. Oganessian, A.G. Popeko, A.V. Yeremin, A. D'Arrigo, G. Fazio, G. Giardina, M. Herman, R. Ruggeri, and R. Sturiale, J. Phys. G **24**, 611 (1998).
- [34] A.V. Ignatyuk, G.N. Smirenkin, A.S. Tishin, Yad. Fiz., **21**, 485 (1975) [Sov. J. Nucl. Phys. **21**, 255 (1975)].
- [35] A.V. Ignatyuk, K.K. Istekov, G.N. Smirenkin, Sov. J. Nucl. Phys. **29**, (1979) 450
- [36] A.J. Sierk, Phys. Rev. C **33**, 2039 (1986).
- [37] P. Grange and H.A. Weidenmüller, Phys. Lett. **96B**, (1980) 26.
- [38] E.M. Rastopchin, S.I. Mulgin, U.V. Ostapenko, V.V. Pashkevich, M.I. Svirin, G.N. Smirenkin, Sov. J. Nucl. Phys. **53**, (1991) 741.
- [39] H.A. Kramers, Physica **7**, (1940) 284.
- [40] C. Bhattacharya, S. Bhattacharya, and K. Krishan, Phys. Rev. C **53**, (1996) 1012.